Title

Sensitivity to direction and velocity of fast frequency chirps in the inferior colliculus of awake rabbit

Abbreviated Title

Frequency-chirp direction and velocity sensitivity in IC

Paul W. Mitchell[a], Kenneth S. Henry[a,b,c], and Laurel H. Carney[a,b]

[a]Departments of Biomedical Engineering, [b]Neuroscience, and [c]Otolaryngology, University of Rochester, Rochester, NY USA

Corresponding author

Laurel H. Carney, Laurel_Carney@URMC.rochester.edu

Abstract

Neurons in the mammalian inferior colliculus (IC) are selective for the direction of fast frequency sweeps (chirps) contained in Schroeder-phase harmonic complexes (SCHR). This selectivity suggests a feature sensitivity in the mammalian IC to fast-chirp direction and velocity. Here, we introduced a novel stimulus consisting of aperiodic random chirps (ARCs) to characterize neural sensitivity to chirp direction and velocity in isolation from periodicity. Extracellular, single-unit recordings were made in the IC of Dutch-belted rabbits. SCHR stimuli had a range of velocities and periodicities, and ARC stimuli had matched velocities. Periodicity tuning was characterized using sinusoidally amplitude-modulated (SAM) noise. The prevalence of direction sensitivity and direction bias to chirps in SCHR and ARC responses was quantified,

demonstrating that the majority of IC neurons (90.5%) were selective to SCHR-chirp direction and that sensitivity to the direction of aperiodic chirps was nearly universal (99.6%). Rate-velocity functions were constructed from ARC responses, revealing that neurons were commonly sensitive to the direction of lower-velocity (0.40 – 1.59 kHz/ms) chirps and were insensitive to the direction of higher-velocity chirps (3.16 – 9.24 kHz/ms). ARC and SAM noise responses were combined using a generalized linear model (GLM) to predict SCHR response rates. The GLM analysis revealed that both velocity and periodicity cues were required to explain SCHR responses. In general, velocity cues had a stronger effect on responses for harmonic stimuli with lower fundamental frequencies. This result has implications for neural encoding of complex sounds that combine envelope periodicities and frequency-sweeps.

Significance

Complex sounds such as speech and music contain fast frequency sweeps (chirps). Recently, responses to a stimulus with well-controlled periodic chirps, the Schroeder-harmonic complex (SCHR), have revealed diverse patterns of selectivity for the direction and velocity of chirps in the inferior colliculus. We studied the interaction between periodicity tuning and chirp selectivity underlying SCHR responses. Using a novel, aperiodic chirp stimulus, we demonstrate through rate-velocity functions that selectivity to chirp direction and velocity is commonly observed even for single chirps. Both neural velocity tuning and periodicity tuning are necessary to predict neural SCHR response rates. The diversity of the observed selectivity challenges models for SCHR selectivity based on cochlear phase dispersion.

Introduction

The inferior colliculus (IC) receives convergent excitatory and inhibitory inputs from several auditory brainstem nuclei, resulting in a variety of complex response properties including frequency tuning (Davis, 2005), sensitivity to interaural differences (Yin et al., 2019), duration

tuning (Casseday et al., 1994), and modulation tuning for amplitude modulation (AM) (Langner and Schreiner, 1988; Krishna and Semple, 2000). Sensitivity of IC neurons to frequency-modulated (FM) sweep direction and velocity has also been studied. Studies of bat IC responses report neurons that prefer, or even respond exclusively, to a selected FM direction, a possible adaptation for echolocation (Suga, 1965; Fuzessery, 1994; Fuzessery and Hall, 1996; Gordon and O'Neill, 1998; Pollak et al., 2011). Additionally, sounds with time and frequency modulations having statistics comparable to those of spectral-peak, or formant-frequency, transitions in sounds including animal vocalizations or speech, have been used to characterize IC spectrotemporal receptive fields (STRFs) in cats and bats (Escabí and Schreiner, 2002; Escabí et al., 2003; Andoni et al., 2007).

Recently, IC FM sensitivity to the direction and velocity of FM sweeps has been explored in anesthetized gerbils (Steenken et al., 2022) and awake budgerigars (Henry et al., 2023). These studies used Schroeder-phase (SCHR) harmonic complexes, an advantageous stimulus for studying FM. The harmonic components of SCHR stimuli have flat magnitude spectra and curved phase spectra that create stimuli with maximally flat envelopes (Schroeder, 1970). The phase differences across harmonic components result in linear frequency sweeps within each fundamental period, extending from the lowest component, typically the fundamental frequency, F0, to the highest harmonic component. SCHR sensitivity is notable for the sheer speed of the FM, with sweeps traveling from F0 to the maximum harmonic (here, 16 kHz) over the fundamental period (here, between 2.5 and 20 ms). The resulting velocities are faster than commonly considered FM signals, such as formant transitions (Liberman and Mattingly, 1989). We report sensitivity in rabbit IC to the direction and velocity of these fast SCHR sweeps, referred to as SCHR chirps. Rabbits do not produce specialized FM vocalizations (Awan et al., 2014) and therefore presumably lack adaptations for processing fast FM. Instead, rabbits have representative mammalian hearing, with average high-frequency audiometric thresholds among

similarly-sized mammals and low-frequency thresholds similar to humans (Heffner and Masterson, 1980).

IC sensitivity to SCHR chirps is poorly understood. Rate-differences between SCHR direction may be partially explained by the phase-dispersive properties in the cochlea (Recio and Rhode, 2000), which might combine with cochlear compression to result in reduced responses to downward-sweeping SCHR chirps in the auditory nerve (AN), at least for the high-frequency region (Recio, 2001). Chirp selectivity in the IC could also arise in octopus cells of the cochlear nucleus, which are selective to SCHR chirp direction (Lu et al., 2022) and provide inhibition to the IC via the ventral nucleus of the lateral lemniscus (VNLL) (Adams, 1997). Alternatively, chirp selectivity may originate (or be influenced) at the level of the IC by the same or similar mechanisms that give rise to other complex stimulus sensitivities. For instance, IC tuning for periodicity (Langner and Schreiner, 1988; Krishna and Semple, 2000; Nelson and Carney, 2007; Kim et al., 2020) can be explained by the dynamics of inhibitory inputs (Nelson and Carney, 2004). Furthermore, the periodicity of SCHR stimuli may affect estimates of IC sensitivity to these stimuli. Therefore, a new approach is required to separate the influences of periodicity and velocity tuning on responses to SCHR chirps. In this study, we recorded IC responses to both SCHR and aperiodic random chirp (ARC) stimuli to assess velocity sensitivity using stimuli without periodicity. From these responses, we constructed rate-velocity functions (RVFs) which describe the sensitivity to velocity of individual neurons. We also used generalized linear models (GLMs) to predict SCHR-chirp responses based on responses to ARC stimuli and SAM noise and showed that, for most neurons, both periodicity and velocity cues were necessary to accurately predict neural responses to SCHR stimuli.

Methods

Extracellular, single-unit recordings were made in the central nucleus of the IC (ICC) of six female Dutch-belted rabbits (*Oryctolagus cuniculus*). Rabbits were obtained from Envigo

(Denver, PA). The age of the animals during experiments ranged from 1-5 years, during which DPOAEs and IC neural thresholds were used to confirm normal hearing (Whitehead et al., 1992). Animals were removed from the study when their DPOAE magnitudes decreased or neural thresholds increased. All methods were approved by the University of Rochester Committee on Animal Resources.

Recordings

Recordings were made in daily two-hour sessions in sound-attenuated booths (Acoustic Systems, Austin, TX, USA). To prevent head movement of the awake rabbits, a headbar (metal or 3D-printed plastic) was surgically affixed to the skull using stainless-steel screws and dental acrylic. Rabbits were anesthetized using ketamine (66 mg/kg) and xylazine (2 mg/kg), administered intramuscularly, for headbar placement, craniotomy, and electrode placements (below). Rabbits were wrapped in a towel and secured in a custom-made chair to limit movement during recording sessions.

Recordings were made using four tetrodes, each consisting of four 18-μm platinum-iridium epoxy-coated wires (California Fine Wire Co., Grover Beach, CA, USA) and plated with platinum black to obtain impedances of approximately 0.1 – 0.5 MOhms. Tetrodes were surgically implanted in the ICC via a small (~2mm diameter) craniotomy in the top of the skull. Stainless-steel guide tubes protected the tetrodes, which were positioned just dorsal to the ICC and then advanced through the ICC using a manual microdrive (Five-drive, Neuralynx, Inc., Bozeman, MT, USA). Tetrodes were advanced before or after recording sessions. The microdrive and tetrodes were surgically replaced every few months, as needed, to vary the recording location. Neural recordings were made using an RHD recording system (Intan Technologies, LLC., Los Angeles, CA, USA), with Intan software running on a Windows PC.

Stimuli were generated using custom MATLAB code (Mathworks, Natick, MA, USA), a MOTU audio interface (16A, Mark of the Unicorn, Cambridge, MA, USA), and a Benchmark digital-to-analog converter and amplifier (DAC3 HGC, Benchmark Media Systems, Inc., Syracuse, NY, USA). Etymotic ER2 earphones (Etymotic Research, Inc., Elk Grove Village, IL, USA) were used to present sound stimuli via custom ear molds (Hal-Hen Company, Inc., Garden City Park, New York, USA). Prior to every session, stimuli were calibrated using ER-7C probe-tube or ER-10B+ microphones (Etymotic Research, Inc., USA). The calibration curve (magnitude and phase) was included in a pre-emphasis filter that compensated all stimuli for the acoustic system's frequency response.

Action potential times and waveforms were extracted from neural recordings using custom MATLAB applications. To identify single-unit events, the voltage recording was filtered using a 4th-order Butterworth bandpass filter (300 – 3000 Hz). An action potential was identified when the filtered voltage signal exceeded a threshold, defined as four standard deviations of the voltage signal. Action potentials were sorted into clusters, presumed to represent different neurons, using features of the waveforms, primarily the slope of the waveform repolarization (Schwarz et al., 2012). Single-units were identified when less than 2% of the interspike intervals were smaller than 1 ms. Neurons studied in consecutive sessions were considered to be unique only when both tetrode location and response properties changed.

Stimuli

Recording sessions began by presenting wideband (100 Hz – 15 kHz) noise to the two ears to characterize the binaural responses. Noise stimuli were presented to the contralateral ear, ipsilateral ear, and both ears at 3, 13, and 33 dB SPL spectrum level, with 1-s durations and 3 repetitions each. Then, a set of stimuli was presented to define neural response properties, including frequency response maps, modulation transfer functions, SCHR sensitivity, and rate-velocity functions.

To generate frequency response maps, a randomly-ordered sequence of 0.2-s-duration tones at frequencies ranging from 250 Hz – 16 kHz was presented at 13, 33, 53, and 73 dB SPL. Tones were presented either contralaterally or diotically with 10-ms raised-cosine on/off ramps, and were separated by 0.4 s of silence. Each stimulus condition was presented three times. Response maps, plots of average discharge rate vs. frequency at each stimulus level, were used to estimate characteristic frequency (CF), the frequency for which threshold was lowest.

Modulation transfer functions (MTFs) were estimated by computing the average rate in response to 100% sinusoidal amplitude-modulated (AM) noise as a function of modulation frequency, over a range of 2 – 350 Hz. The wideband noise (100 Hz – 10 kHz) was 1 s in duration, including 50-ms raised-cosine on/off ramps, separated by 0.5 s of silence, presented diotically. Modulation frequencies were presented in random order, with 5 repetitions of each. Stimuli were presented at a spectrum level of 33 dB (overall level of 73 dB SPL). MTF categorization was based on criteria that were slightly modified from Kim et al. (2020). MTF types were categorized as band-enhanced (BE) if (1) the MTF had two consecutive points greater than the product of the unmodulated rate (r_{um}) and a criterion K, and (2) the MTF did not have more than one point below the product of r_{um} and $1/K$. Similarly, MTFs were categorized as band-suppressed (BS) if (1) the MTF had three consecutive points less than r_{um}/K, and (2) the MTF did not have more than one point above $r_{um} \times K$. For this study, K was set to 1.2, i.e., a 20% increase in rate with respect to the unmodulated response was required for BE MTFs and a 20% decrease was required for BS MTFs. MTFs that had both enhanced and suppressed bands that met the above criteria were categorized as hybrid MTFs. In the population of neurons studied, 43.3% were BS, 17.0% were BE, 24.5% were hybrid, and 5.2% were flat, and the rest had other MTF shapes including high-pass or low-pass. For BE neurons, the peak of the MTF was designated the best modulation frequency (BMF). For BS neurons, the lowest

point in the MTF was designated the trough modulation frequency (TMF), and for hybrid neurons both a BMF and TMF were identified.

SCHR stimuli were produced using the phase spectrum introduced in Schroeder (1970) (Fig. 1A-D). For a harmonic complex with n components, the phase of the nth component was described by $\theta_n = C\pi n(n+1)/N$, where N is the total number of harmonic components, and C is a scalar that describes the phase-direction and duty cycle of the stimulus. A random

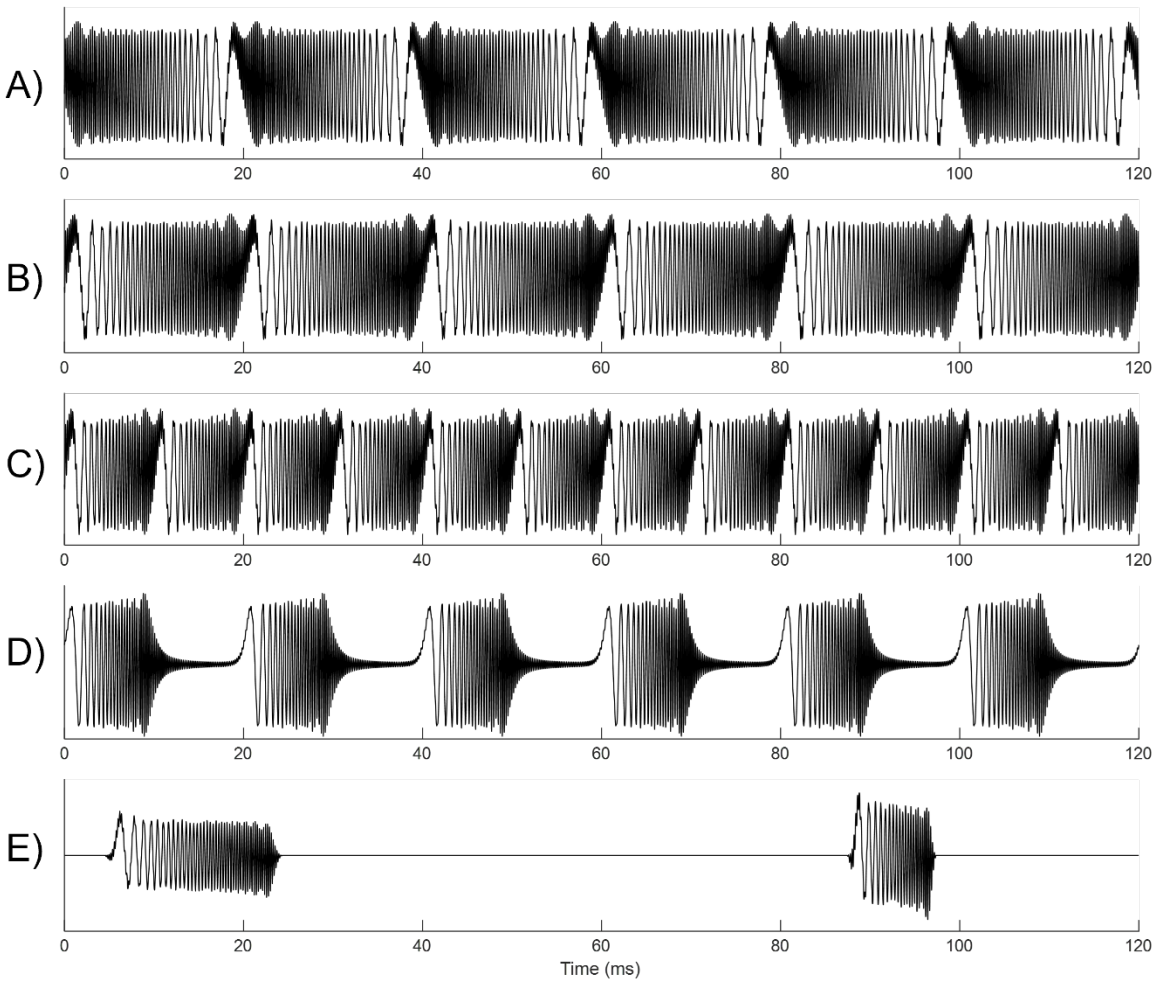

Figure 1 – Stimulus waveforms of SCHR and ARC stimuli. Note that the maximum harmonic in this figure is 5 kHz for clarity; in the actual stimuli, maximum harmonic was 16 kHz. (A) SCHR with F0 = 50 Hz, C = 1. (B) SCHR with F0 = 50 Hz, C = -1. (C) SCHR with F0 = 100 Hz, C = -1. (D) SCHR with F0 = 50 Hz, C = -0.5. (E) Two consecutive ARC-stimulus chirps separated by silence.

sequence of SCHR stimuli was presented, with F0 equal to 50, 100, 200, or 400 Hz, and C equal to -1, -0.5, 0, 0.5, or 1. For all cases, the frequency of the highest harmonic component was 16 kHz. The number of harmonic components, N, depended on F0, and ranged between 40 and 320. Thirty repetitions of each F0 and C combination were presented. Stimuli were presented diotically at 63 dB SPL, with a duration of 0.4 seconds, 0.6 seconds of silence between stimuli, and 25-ms raised cosine on/off ramps. Average discharge rates over the stimulus duration were calculated for each F0 and C combination. Receiver-operating-characteristic (ROC) analysis (Egan, 1975) was used to evaluate neural direction selectivity between SCHR conditions with equivalent F0 and C-values of opposite signs (i.e. F0 = 50 Hz, C = ±1). Neurons were deemed significantly biased toward one sweep direction if the area under the ROC curve (AUC) was above 70.7% or below 29.3%. Additionally, the direction of the bias was designated negative for neurons with AUCs above 70.7% (indicating greater mean response rate for the negative Schroeder stimulus) and positive for neurons with AUCs below 29.3%. The ROC threshold of 70.7% (and 29.3%) was chosen because it is equivalent to the targeted level on the psychometric function by a two-down, one-up psychophysical procedure (Levitt, 1971).

Rate-velocity functions (RVFs) were based on responses to ARC (aperiodic random chirp) stimuli. ARC stimuli were isolated SCHR chirps, or single fundamental periods extracted from a SCHR stimulus, equivalent to one full SCHR chirp spanning F0 to the maximum harmonic, or vice versa (Fig. 1E). To produce the stimulus waveforms, first, we generated a random sequence of chirp velocities that were equivalent to SCHR F0s of 25, 50, 100, 200, 400, and 600 Hz. Chirp direction (upward or downward) was also randomly varied across stimuli. These parameters together resulted in ARCs with velocities ±0.40, ±0.80, ±1.59, ±3.16, ±6.24, and ±9.24 kHz/ms. Each combination of velocity and direction was presented a total of 42 times within each full stimulus, in random order. ARCs were randomly spaced to avoid periodicity,

using 40 – 60 ms uniformly distributed inter-chirp intervals. The full stimulus set was presented 20 times. Each individual chirp had raised-cosine on/off ramps, each with duration equivalent to 10% of chirp duration. Chirps were presented diotically at a sound level equal to $68\ dB\ SPL - 10 \times \log_{10}(T/T_{ref})$, where T is the duration of the chirp, and T_{ref} = 2.5 ms (the duration of a SCHR chirp with F0 = 400 Hz). This scaling ensured that energy was equivalent across chirps of different durations. Extracting response rates from ARC-stimulus responses was complicated by variation in onset response latency and the presence of offset responses in many neurons. The response-rate calculation began by locating the peak rate in the peristimulus time histogram (PSTH) over a time window starting at chirp onset with a duration matched to that of the chirp plus the minimum spacing between chirps (i.e., chirp duration + 40 ms) (Fig. 2). Then, response rate was calculated by summing spikes over a 20-ms time window centered at the peak of the PSTH, except where this window would cross the minimum (0 ms) or maximum (chirp duration + 40 ms) of the PSTH time axis. ROC analysis of ARC rates was performed in an identical manner as for SCHR rates. ARC rates were used to generate RVFs, which described how a neuron's rate changed as a function of chirp velocity (Figs. 3-7). The RVF describes a neuron's response profile to aperiodic chirps of different velocities, allowing salient response properties to be easily identified.

Analysis

Principal Component Analysis (PCA) was performed on the RVFs using the MATLAB function PCA (2021b, MathWorks) on the set of RVFs (247 in total). RVFs were normalized by their individual peak rates before PCA analysis. SCHR responses were predicted based on MTFNs and RVFs using generalized linear models (GLMs) (Nelder and Wedderburn, 1972). First, SCHR rates, MTFNs, and RVFs were normalized by each of their maximum rates. For the responses to periodic stimuli, (MTFN and SCHR), cycle rate was used, defined as the average rate per fundamental period (T0). Cycle rate (spikes/cycle) was used to counteract the strong

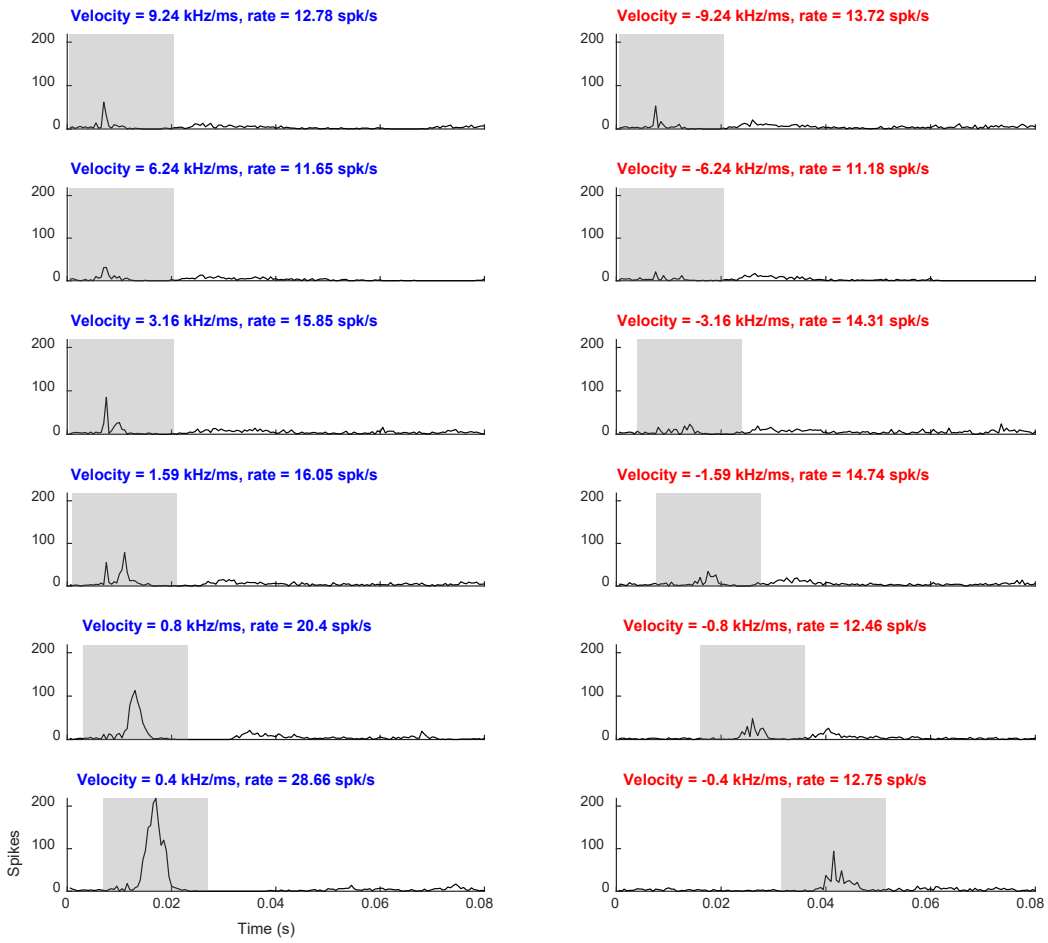

Figure 2 – A visual depiction of ARC-stimulus rate calculation. Black lines illustrate PSTHs (bin size = 0.5 ms) of responses to ARCs of different velocities. The left column (blue titles) contains positively-sloped ARCs (equivalent direction to −SCHR chirps), and the right column (red titles) contains negatively-sloped ARCs (equivalent direction to +SCHR chirps). The shaded rectangles indicate the placement of the 20-ms window over which response rate is calculated. Generally, the window is centered at the peak of the PSTH, except where that would cause the window to cross the minimum (0 ms) or maximum (80 ms) time intervals (e.g. velocity = 9.24 kHz/ms PSTH, top left).

phase-locking of many neurons to the fundamental frequency, which resulted in average rates that disproportionally increased with F0 using the conventional calculation (spikes/second). For the aperiodic stimulus (ARC), rate was calculated using the previously mentioned method of summing spikes over a window up to 40-ms in duration centered around the peak of the PSTH.

MTFNs and RVFs were then projected onto the SCHR space such that each of the 16 SCHR rates was associated with one point on the MTFN and one point on the RVF. The SCHR rates can be visualized as a surface on this periodicity/velocity grid. The periodicity and velocity of each SCHR point on this grid was matched with the closest available modulation frequency and velocity from the MTFN and RVF, respectively (data were not interpolated), creating a feature vector for the neurons' pure response to periodicity and velocity changes. Then, a relationship between the periodicity and velocity feature vectors and SCHR rates was defined for the GLM as follows:

$$R_S = b_P R_P + b_V R_V + b_I (R_P * R_V) + b_0 \quad , \qquad \text{(Eqn. 1)}$$

where R_P and R_V refer to rates of the periodicity and velocity feature vectors, respectively. R_S is the predicted response to SCHR stimuli in cycle rate, and b_n are the GLM coefficients. There were three terms in the GLM—a periodicity term, a velocity term, and an interaction term. GLM coefficients were estimated using the MATLAB function glmfit (2021b, MathWorks), with the distribution argument set to *normal* and constant argument set to *on*. The GLM coefficients were b_P, the periodicity coefficient, b_V, the velocity coefficient, b_I, the interaction term coefficient, and b_0, a constant. After the SCHR rate prediction was calculated using estimated coefficients, the coefficient of determination (R^2) of the predicted and recorded SCHR cycle rates was determined to assess prediction quality. This process was repeated for two additional, simpler GLMs:

$$R_S = b_1 R_P + b_0 \quad , \text{ and} \qquad \text{(Eqn. 2)}$$

$$R_S = b_1 R_V + b_0 \quad . \qquad \text{(Eqn. 3)}$$

These simpler GLMs depended only on one feature vector and thus could be used to assess the importance of periodicity or velocity alone. The coefficients of determination (R^2) of these

265 two model predictions were obtained and used to measure the impact of the two features on
266 neurons' SCHR responses.

267 The following equation was used to calculate the contribution of velocity-cues to the total
268 explainable variance:

269 $$Percent\ contribution\ of\ velocity\ to\ R^2 = \frac{\left(R^2{}_{combined} - R^2{}_{periodicity}\right)}{R^2{}_{combined}} \times 100\ , \qquad \text{(Eqn. 4)}$$

270 where $R^2{}_{combined}$ and $R^2{}_{periodicity}$ refer to the coefficient of determination of the combined
271 model (Eqn. 1) and periodicity-alone model (Eqn. 2), respectively. Equation 4 allowed the
272 amount of additional variance explained by the inclusion of velocity (either in the velocity term or
273 interaction term in Eqn. 1) to be directly quantified.

274 **Results**

275 **A.** Sensitivity of IC neurons to direction and velocity of SCHR chirps was diverse

276 Data were recorded over a span of 330 sessions and included recordings from 335
277 unique single units. Response properties of single-unit neurons are illustrated using RMs,
278 MTFs, RVFs, and raster plots of SCHR responses (Figs. 3-7). The neural sensitivity to chirps is
279 illustrated in the SCHR raster plots, which illustrate salient trends in the responses of each
280 neuron, such as detailed timing and rate differences between SCHR conditions that differ in
281 direction or velocity. RMs were used to determine CF; these plots also reveal off-CF inhibitory
282 regions. MTFs were categorized as BE, BS, or hybrid, and were used to identify BMF and/or
283 TMF. Lastly, RVFs were constructed from ARC-stimuli responses, which differ from SCHR
284 responses because they reflect the neural sensitivity to velocities of single chirps removed from
285 a periodic context. Altogether, RMs, MTFs, and RVFs provided a response profile from which
286 underlying mechanisms of SCHR-chirp sensitivity were hypothesized—specifically, that SCHR
287 responses were the result of a combination of modulation tuning, off-CF inhibition in the RM,

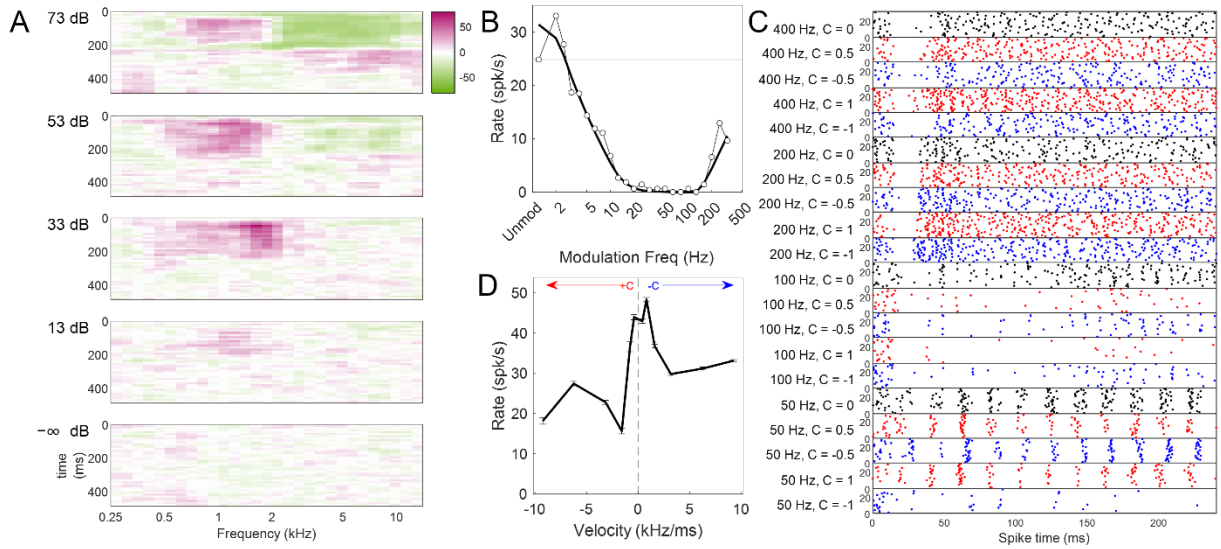

Figure 3 – Responses of unit R24TT4P7N2 to characterizing stimuli. (A) Response Map – Panels are arranged vertically by sound level of pure tones. Color plots reflect response rate versus frequency (x-axis) and time following tone onset (y-axis); magenta regions have increased activity relative to spontaneous rate, and green regions have decreased activity relative to spontaneous rate. (B) Modulation Transfer Function – rate versus modulation frequency. The solid black line is smoothed from raw data (shown as circular points). Grey horizontal line reflects unmodulated rate. (C) Dot raster plots of SCHR responses – Panels are arranged vertically by SCHR condition (F0 and C-value pairs). Within panels, rows of dots reflect repetitions (30 each). Responses to negative C-values (−SCHR) are plotted with blue dots, and positive C-values (+SCHR) with red dots. Black is used for C = 0. For rows with C = ±1, F0s of 50, 100, 200, and 400 Hz correspond to chirp velocity magnitudes of ±0.80, ±1.59, ±3.16, and ±6.24 kHz/ms, respectively. For rows with C = ±0.5, F0s of 50, 100, 200, and 400 Hz correspond to chirp velocity magnitudes of ±1.59, ±3.18, ±6.32, and ±12.48 kHz/ms, respectively. For rows with C=0, chirp velocity was infinite. (D) Rate-velocity function – constructed using responses to ARC-stimuli. Colored arrows mark the SCHR C-values of chirps of equivalent direction. Error bars are the standard error of rates across repetitions (20 each).

and chirp velocity tuning, with the relative importance of these influences differing between neurons. Figures 3-7 provide several diverse examples that demonstrate how the SCHR

304 response profile of a given neuron may be influenced by a combination of modulation tuning,
305 chirp velocity tuning, and off-CF inhibition.

306 Figure 3 shows an example of a unit with a complex SCHR response that was not fully
307 explainable by the responses to characterizing stimuli. The SCHR dot raster plot (Fig. 3C)
308 displays stronger rates in response to positive-chirps (red dots) at the lowest chirp velocity, 50
309 Hz, C = ±1. This positive-chirp preference was not maintained for higher velocities. The
310 neuron's MTF (Fig. 3B) was BS, with a trough spanning modulation frequencies that included
311 the SCHR F0s of 50 and 100 Hz, and with relatively less suppression at modulation frequencies
312 matching the F0s of 200 and 400 Hz. If the MTF solely predicted this neuron's SCHR response,
313 responses to 50- and 100-Hz SCHR chirps should have been nearly entirely suppressed.
314 However, the neuron's response was robust for all 50-Hz chirp conditions except for 50 Hz, C =
315 -1, suggesting that the direction and/or velocity sensitivity to these chirps overcame the
316 suppression observed in the MTF. Thus, the MTF alone could not simply explain this neuron's
317 SCHR response profile. Meanwhile, the RM (Fig. 3A) was sharply tuned to 1.2 kHz with a low
318 threshold (13 dB SPL), and revealed a high-frequency inhibitory region at high sound levels with
319 a long duration and shorter latency than the excitation at CF. If the neuron's SCHR response
320 were dependent on this asymmetrical sideband inhibition, the long-duration inhibition would
321 suppress the coincident excitation during downward chirps, resulting in a stronger response to
322 upward chirps (i.e., –SCHR) than to downward chirps (Gordon and O'Neill, 1998). However, the
323 neuron instead responded more strongly to +SCHR (downward) chirps than to –SCHR (upward)
324 for 50-Hz F0. Therefore, the neuron's asymmetrical sideband inhibition alone could not explain
325 the SCHR response. The neuron's RVF (Fig. 3D) shows an increased response to upward-
326 sweeping chirps (−SCHR, blue) compared to downward-sweeping chirps (+SCHR, red) for most
327 velocity-pairs, with the exception of ±0.40 kHz/ms (equivalent to SCHR with F0 = 25 Hz, C =
328 ±1), for which rates were slightly higher for the downward-sweeping chirp. For the most part, the

329 RVF also did not adequately explain SCHR responses; that is, SCHR rates did not consistently
330 favor upward chirps (−SCHR). Instead, direction selectivity was only strong at 50 Hz, C = ±1,
331 showing a selectivity for downward SCHR chirps (+SCHR), while the RVF showed a selectivity
332 for upward chirps for the equivalent velocity pair (±0.80 kHz/ms). That the RM, MTF, nor RVF
333 simply predict the SCHR response suggests that the SCHR response may have been driven by
334 an interaction between these three feature sensitivities.

335 Another example neuron, illustrated in Fig. 4, had a BE MTF, and a RM dominated by
336 excitation, with a CF of 2 kHz. This neuron's raster plot for SCHR responses showed relatively
337 greater responses to +SCHR chirps for all chirp pairs, with the exception of 400-Hz SCHR
338 stimuli, which were comparatively direction-neutral. Also notable is the suppressed response to
339 400-Hz SCHR relative to other F0s.

340 Figure 5 shows responses of an example neuron with a BE MTF and a RM similarly
341 dominated by excitation, with a CF of 2.3 kHz. However, this neuron was –SCHR selective for
342 nearly all chirp pairs, with the exception of 400-Hz SCHR. Thus, neurons with the same MTF
343 type could have opposing chirp-direction selectivity. Again, the MTF shape alone did not predict
344 SCHR responses. Additionally, neither of the neurons in Figs. 4 and 5 had RMs with inhibitory
345 regions, although the low spontaneous rates of these neurons likely prevented the RMs from
346 showing inhibition. However, there was also no evidence for inhibition from either ear based on
347 the neurons' binaural noise responses; for example, adding ipsilateral noise did not suppress
348 responses to contralateral noise. Finally, these neurons both had RVFs that were consistent
349 with the SCHR rate profiles. In Fig. 4, downward-sweeping chirps elicited a higher response rate
350 than upward-sweeping ones for every velocity-pair. In Fig. 5, the responses to upward-sweeping
351 chirps were larger to all velocity-pairs, except for ±6.24 kHz/ms (equivalent to 400 Hz) —
352 interestingly, the selectivity for −SCHR seen for other SCHR conditions in the dot raster plot
353 was absent for the 400-Hz pair for both neurons.

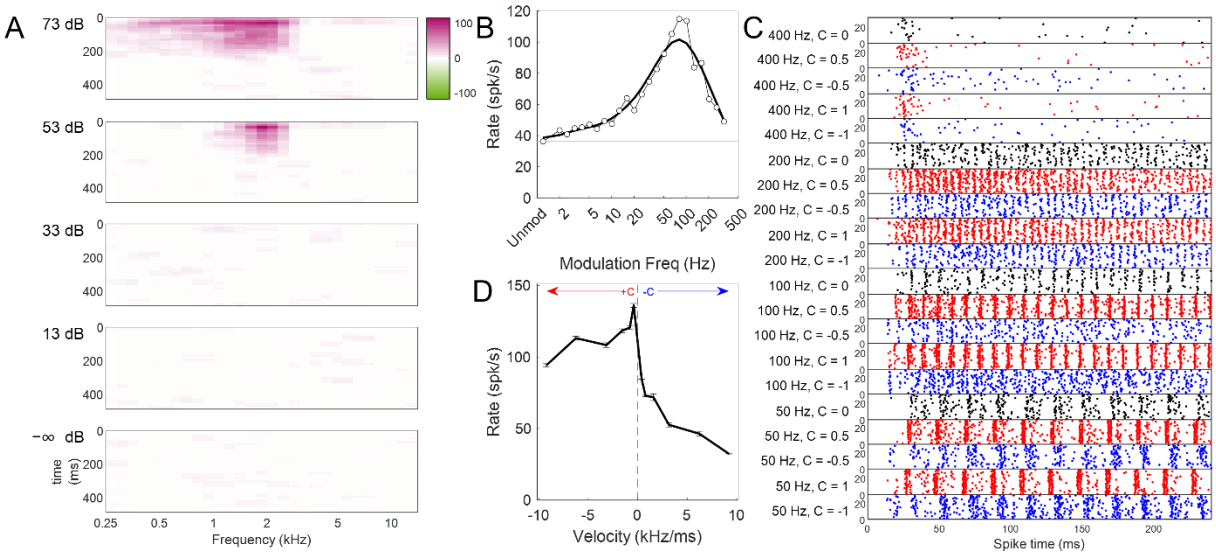

Figure 4 – Responses of unit R24TT2P8N4 to characterizing stimuli. (A) Response Map, (B) Modulation Transfer Function, (C) SCHR dot-raster plot, (D) Rate-Velocity Function. Figure description identical to Fig. 3.

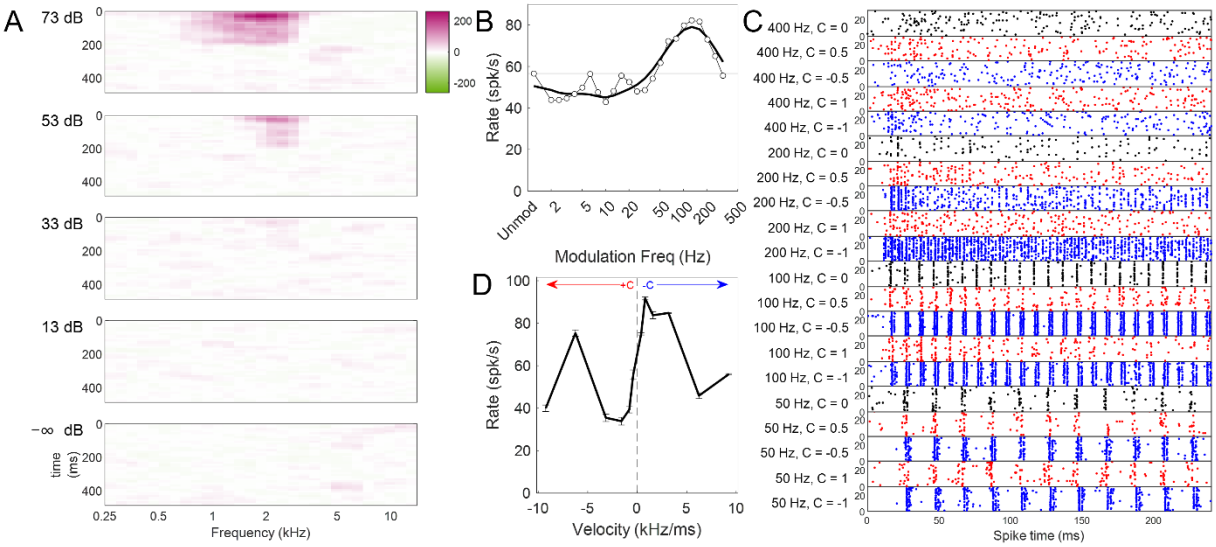

Figure 5 – Responses of unit R25TT2P5N1 to characterizing stimuli. (A) Response Map, (B) Modulation Transfer Function, (C) SCHR-dot raster plot, (D) Rate-Velocity Function. Figure description identical to Fig. 3.

Figure 6 shows responses of a neuron with a flat MTF that was also selective for –SCHR chirps for low-F0 chirp pairs. This figure illustrates that neurons that were neither BE nor BS

could still be sensitive to the direction of SCHR chirps, providing further evidence that SCHR sensitivity was not a property tied to a particular MTF type.

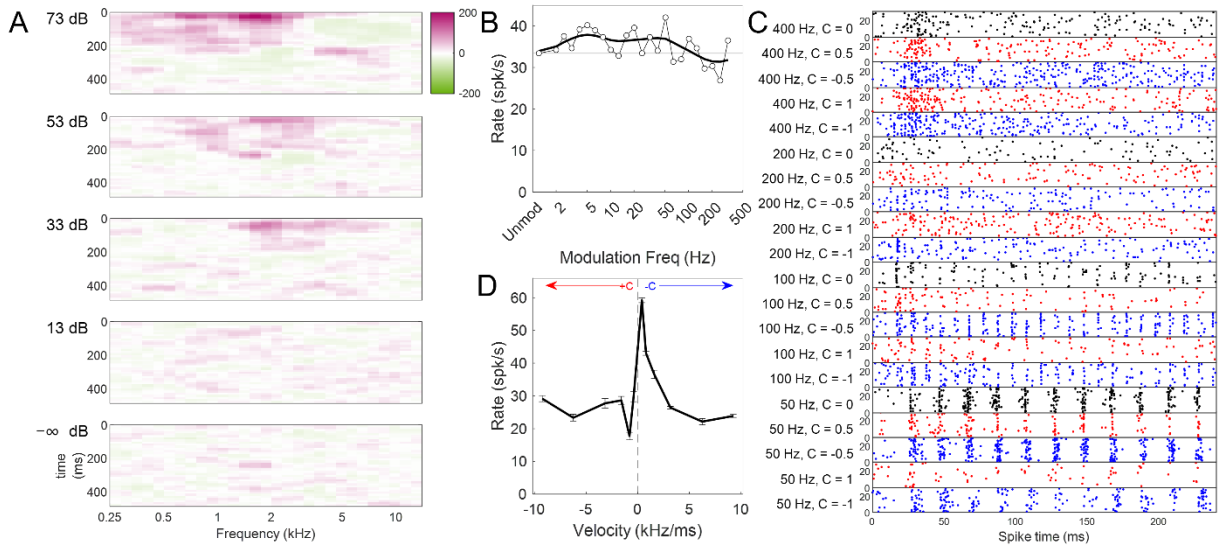

Figure 6 – Responses of unit R24TT2P8N3 to characterizing stimuli. (A) Response Map, (B) Modulation Transfer Function, (C) SCHR dot-raster plot, (D) Rate-Velocity Function. Figure descriptions identical to Fig. 3.

Figure 7 shows responses of an example neuron with an RM that had a low-frequency inhibitory region at high tone levels. This inhibition appears to slightly lag the excitatory region around CF—according to the prediction based on asymmetric inhibition, an upward sweep should result in a coincidence of inhibition and excitation, resulting in selectivity towards downward chirps (i.e., +SCHR). However, the dot-raster plots of the neuron responses to SCHR stimuli show a selectivity towards upward chirps (–SCHR). Figures 3 and 7 are examples for which chirp selectivity did not agree with the prediction made by the asymmetric inhibitory-sideband theory (Fuzessery and Hall, 1996; Gordon and O'Neill, 1998) and suggest that sideband inhibition alone could not predict SCHR responses.

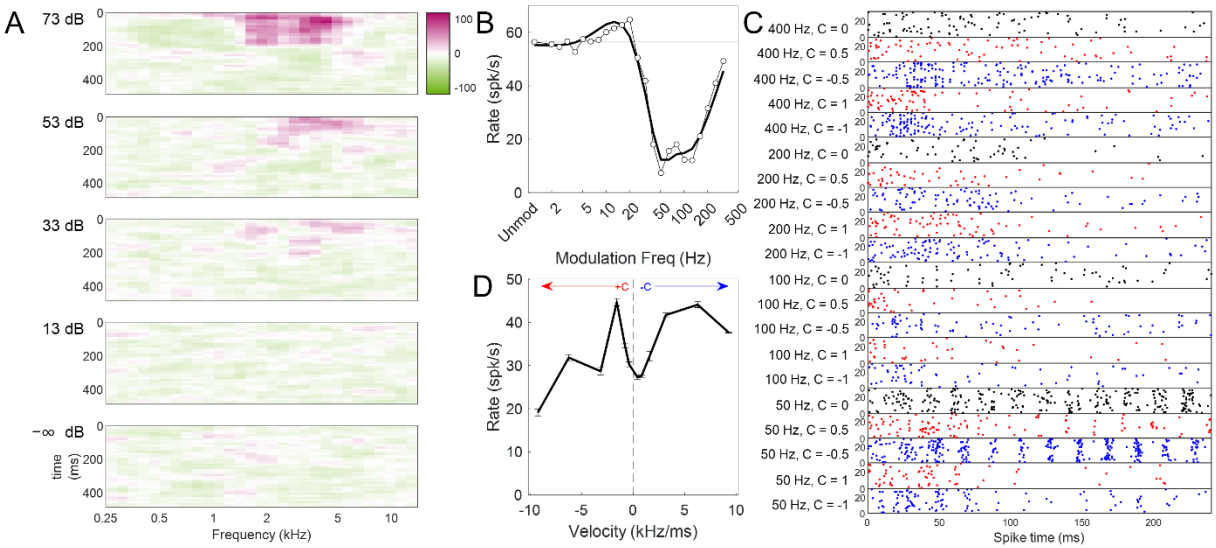

Figure 7 – Responses of unit R24TT1P9N2 to characterizing stimuli. (A) Response Map, (B) Modulation Transfer Function, (C) SCHR dot raster plot, (D) Rate-Velocity Function. Figure description identical to Fig. 3.

These example neurons illustrate the diversity of response profiles to SCHR chirps in the IC. Conventional IC features, such as modulation tuning and off-CF inhibition observed in RMs, could not fully explain the responses to SCHR chirps. This observation led to the hypothesis that sensitivity to the chirp velocity contributed to SCHR-chirp sensitivity. This hypothesis served as the motivation for the ARC stimulus, which allowed variation of the velocity cue. RVFs based on ARC-stimulus responses often reflected the rate profiles seen in SCHR dot-raster plots (e.g., Figs. 4,5, and 6), but sometimes did not (e.g., Figs. 3 and 7), suggesting that while many SCHR responses could be explained by their RVFs, others required a more complex interaction between multiple feature sensitivities.

B. The majority of IC neurons were selective for SCHR direction

After establishing that individual IC neurons in awake rabbit displayed sensitivity for SCHR-chirp direction, this property was quantified for the population of recorded neurons. SCHR-direction sensitivity was quantified within a given F0 and pair of opposite-signed C values

by performing ROC analysis on response rates for SCHR-sign pairs. Neurons for which responses to SCHR-sign pairs allowed direction to be discriminated 70.7% of the time via the ROC test were labeled direction-sensitive.

In total, SCHR responses were recorded from 157 neurons. In Table 1, the *Overall* column shows the percentage of all neurons that were direction selective for each F0 and C condition, or for at least one combination (i.e., Table 1, *Any* row). Direction selectivity was more common for lower F0s and generally was less common for higher F0s

F0 (Hz)	C-Value	Overall (n = 157)	BE (n = 31)	BS (n = 59)	Hybrid (n = 41)	Low CF (n = 36)	Mid CF (n = 39)	High CF (n = 82)
50	±1	53.5	74.2	45.8	51.2	58.3	61.5	47.6
	±0.5	59.2	81.0	47.1	60.0	56.7	73.9	55.6
100	±1	51.0	77.4	44.1	36.6	63.9	61.5	40.2
	±0.5	51.2	66.7	49.0	34.3	50.0	73.9	44.4
200	±1	50.3	67.7	47.5	36.6	63.9	56.4	41.5
	±0.5	35.2	71.4	23.5	22.9	33.3	60.9	27.8
400	±1	49.0	48.4	47.5	51.2	47.2	48.7	50.0
	±0.5	48.8	66.7	41.2	45.7	46.7	56.5	47.2
Any		90.5	93.6	93.2	82.9	97.2	92.3	86.6

Table 1 - Percent of direction sensitive neurons by subgroup as determined by ROC analysis of SCHR responses. Neurons are sorted into subgroups by MTF shape and CF. Neurons with CF less than 6 kHz were labeled "Low CF", and neurons with CF greater than 6 kHz were labeled "High CF". Direction sensitivity was quantified for each F0/C condition. The percentage of neurons sensitive for any F0/C condition was also determined, defined as neurons that were sensitive to sweep direction for at least one F0/C condition.

For a given F0, the C = ±0.5 condition had a chirp velocity equivalent to the 2F0 and C = ±1 condition. However, these equivalent-velocity pairs often differed in prevalence of direction

406 selectivity (i.e., 200 Hz, C = ±0.5 and 400 Hz, C = ±1, *Overall* column). This result suggested
407 that prevalence of direction selectivity did not depend solely on chirp velocity and was possibly
408 also influenced by SCHR periodicity or duty cycle.

409 Finally, 90.5% of neurons were direction selective for at least one F0 and C condition
410 (Table 1, *Any* row), demonstrating that SCHR chirp direction selectivity was nearly ubiquitous.
411 To determine the proportion of neurons expected to be selective for any SCHR condition by
412 random chance, responses to either direction were shuffled within each SCHR-sign pair for
413 each neuron. ROC tests were then performed on these shuffled responses, and the neurons
414 that were direction selective for at least one F0/C condition were tallied as before. After shuffling
415 the responses 1000 times, 3.2% of the neurons were selective for at least one F0/C condition
416 (with a standard deviation of 2.6%), suggesting that the threshold used in the ROC test
417 (70.07%) was sufficiently high.

418 **C.** MTF shape, but not CF, was related to prevalence and direction of SCHR selectivity

419 The prevalence of SCHR-direction selectivity depended on F0. Hence, it was relevant to
420 quantify the extent to which modulation sensitivity could influence SCHR responses. To
421 examine the effect of MTF shape on SCHR direction selectivity, results of an ROC analysis are
422 shown in Fig. 8. BE neurons were significantly more direction selective than BS neurons for 5
423 SCHR conditions, and more direction selective than Hybrid neurons for 5 conditions, suggesting
424 that BE neurons were more often direction selective than other MTF shapes (χ^2 test of
425 independence, Fig. 8 caption. Additionally, for several SCHR conditions (e.g., 50 Hz, C = ±1; 50
426 Hz, C = ±0.5; 400 Hz, C = ±0.5) a notably larger percentage of BE neurons were +SCHR
427 selective than for the rest of the MTF shapes, suggesting that BE neurons were more likely than
428 neurons of other MTF types to be +SCHR selective. For most SCHR conditions, all MTF types
429 tended to have more –SCHR selective neurons. However, for all but one MTF group and SCHR

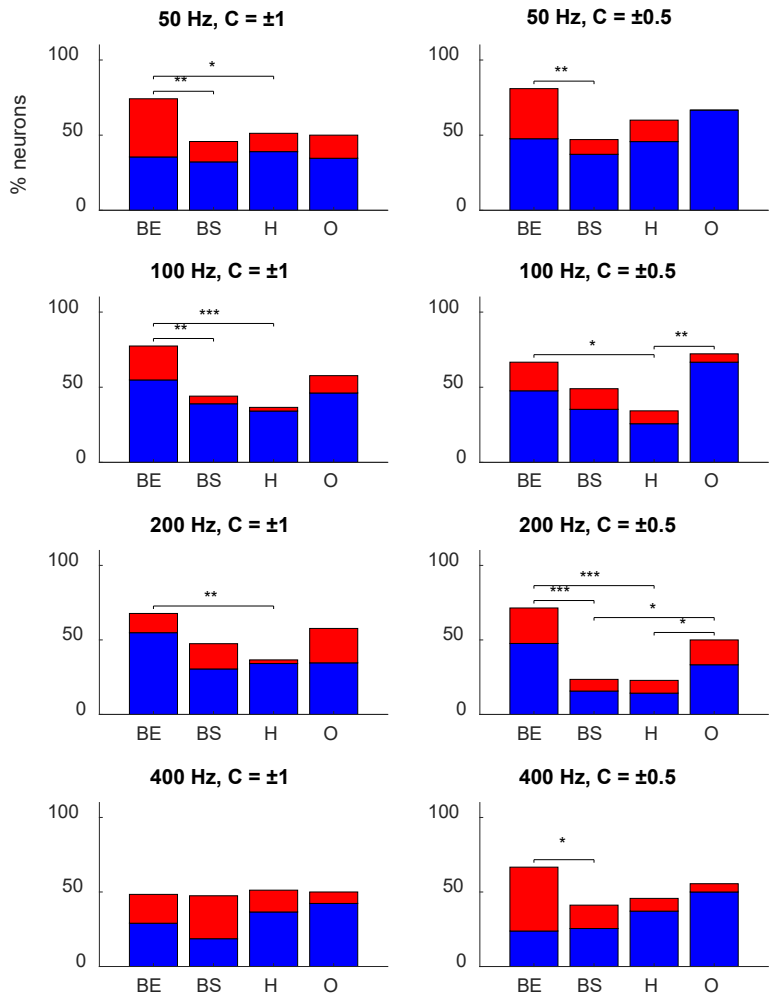

Figure 8 - Percent of direction selective neurons determined by ROC analysis for different MTF shapes, by SCHR condition (BE – Band-Enhanced, BS – Band-Suppressed, H – Hybrid, O – Other). Blue bar-segments correspond to –SCHR selective neurons, and red bar-segments correspond to +SCHR selective neurons. Brackets indicate significant differences of direction selectivity prevalence between groups, as determined by the χ^2 test of independence, with asterisks indicating the level of significance ($p < 0.05$, ** $p < 0.01$, *** $p < 0.001$). Precise p-values are reported here for each panel. 50 Hz, C = ±1—BE-BS, $p = 0.0099$; BE-H, $p = 0.0477$. 50 Hz, C = ±0.5—BE-BS, $p = 0.0083$. 100 Hz, C = ±1—BE-BS, $p = 0.0025$; BE-H, $p = 0.0006$. 100 Hz, C = ±0.5—BE-H, $p = 0.0187$; H-O, $p = 0.0088$. 200 Hz, C = ±1—BE-H, $p = 0.0088$. 200 Hz, C = ±0.5—BE-BS, $p = 0.0001$; BE-H, $p = 0.0003$; BS-O, $p = 0.0359$; H-O, $p = 0.0450$. 400 Hz, C = ±0.5—BE-BS, $p = 0.0492$.*

condition (*Other*, 50 Hz, C = ±50 Hz), both positively- and negatively-selective neurons appeared. Interestingly, despite the large differences between BE and BS groups within individual SCHR conditions, the percentage of neurons in each group that were direction selective at any SCHR condition (Table 1, bottom row) were similar. This result shows that BS neurons were more frequently selective only at a few SCHR conditions compared to BE neurons. Indeed, the average number of selective SCHR conditions among BE neurons was 4.6, compared to 3.2 conditions on average for BS neurons. Hybrid neurons were selective for 3.1 conditions on average. Overall, the prevalence of direction selectivity among BE, BS, and hybrid neurons was high, with hybrid neurons having the lowest prevalence.

To examine the effect of CF on SCHR-direction selectivity, results of an ROC analysis for different CF ranges are shown in Fig. 9. The relationship of prevalence of selectivity and CF is less clear than for MTF shape. Generally, low-CF and mid-CF neurons were more often selective than high-CF neurons, but this trend varied by SCHR condition. Generally, most CF groups had more –SCHR selective neurons for all SCHR conditions. Generally, mid-CF neurons displayed robust –SCHR selectivity compared to high-CF neurons, which were more +SCHR selective. Low-CF neurons may have been more selective for –SCHR at low F0s, but become more balanced at higher F0s. Overall, much like MTF groups, all CF groups had both positive- and negative-selective neurons. Also, like the MTF groups, all CF groups had an overall high percentage of direction selectivity (Table 1, *Any* row).

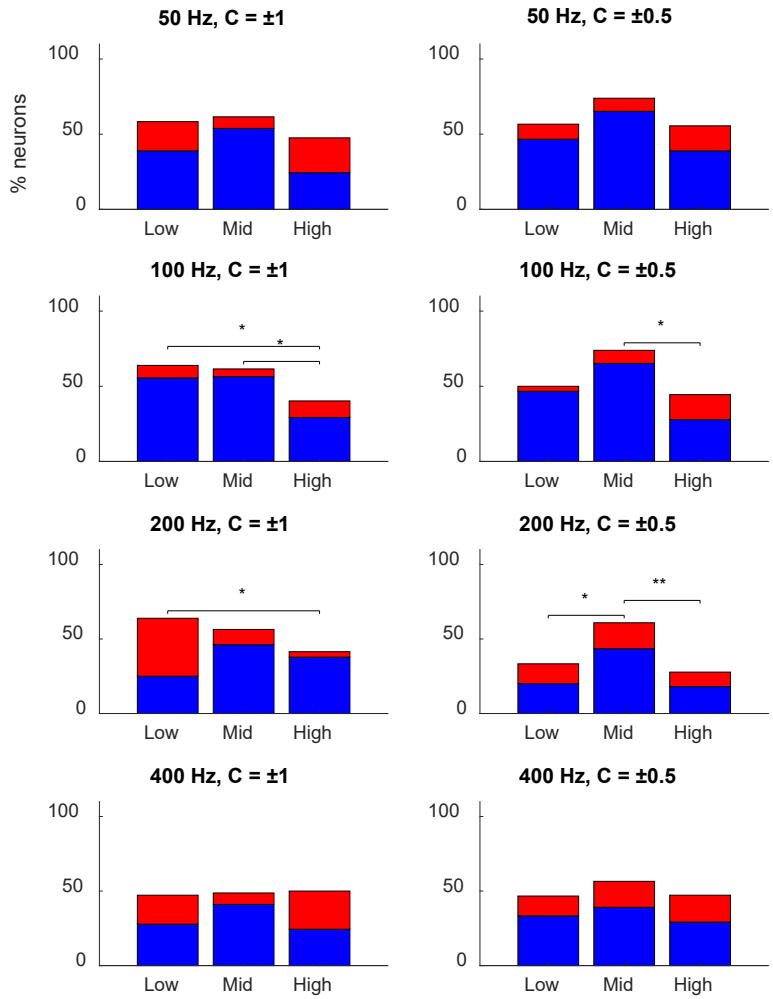

Figure 9 - Percent of direction selective neurons determined by ROC analysis for different CF ranges, low (<3 kHz), mid (>3 kHz and <6 kHz), and high (>6 kHz), by SCHR condition. Blue bar-segments correspond to –SCHR selective neurons, and red bar-segments correspond to +SCHR selective neurons. Brackets indicate significant differences of direction selectivity prevalence between groups, as determined by the χ^2 test of independence, with asterisks indicating the level of significance ($p < 0.05$, ** $p < 0.01$, *** $p < 0.001$). Precise p-values are reported here for each panel. 100 Hz, C = ±1—Low-High, $p = 0.0179$; Mid-High, $p = 0.0283$. 100 Hz, C = ±0.5—Mid-High, $p = 0.0138$. 200 Hz, C = ±1—Low-High, $p = 0.0248$. 200 Hz, C = ±0.5—Low-Mid, $p = 0.0459$; Mid-High, $p = 0.0040$.*

468 **D**. Direction selectivity to ARC stimuli was near-ubiquitous

469 ROC analysis was performed on responses to ARC stimuli to determine the prevalence of
470 direction selectivity of neurons in the absence of periodicity. Similar to the analysis performed
471 for SCHR responses (Table 1), equivalent ARC chirp speeds were paired, and pairs for which
472 the chirp direction could be discriminated 70.7% of the time via ROC test were labeled direction-
473 selective.

474 ARC responses were collected from 247 neurons (Table 2). As for the SCHR ROC
475 results, direction selectivity to ARC stimuli was common for faster chirp velocities and became
476 increasingly uncommon as velocity increased. When comparing equivalent chirp-velocity
477 conditions between SCHR and ARC-stimulus responses (e.g., 0.80 kHz/ms ARC chirp and 50-
478 Hz SCHR, etc.), neurons were more commonly selective for ARC chirps than for their SCHR

Velocity (kHz/ms)	Overall (n = 247)	BE (n = 33)	BS (n = 115)	Hybrid (n = 67)	Low CF (n = 90)	Mid CF (n = 36)	High CF (n = 121)
±0.40	80.2	90.9	80.9	71.6	85.6	86.1	74.4
±0.80	72.9	78.8	72.2	67.2	78.9	69.4	69.4
±1.59	73.3	87.9	73.9	73.1	76.7	75.0	70.2
±3.16	62.3	69.7	53.9	71.6	57.8	55.6	67.8
±6.24	56.3	63.6	53.9	61.2	53.3	38.9	63.6
±9.24	52.2	48.5	47.8	61.2	46.7	52.8	56.2
Any	99.6	100	100	98.5	100	100	99.2

479 *Table 2 – Percent of direction selective neurons by subgroup as determined by ROC analysis of ARC-stimulus*
480 *responses. Neurons are sorted into subgroups by MTF shape and CF. Neurons with CF less than 6 kHz were labeled*
481 *"Low CF", and neurons with CF greater than 6 kHz were labeled "High CF". Direction selectivity was quantified for*
482 *each F0/C condition. The percentage of neurons selective for any F0/C condition was also determined, defined as*
483 *neurons for which at least one F0/C condition was selective.*

484 counterparts. Finally, 99.6% of neurons were direction selective for at least one ARC velocity
485 (Table 2, *Any* row). Stated differently, only one neuron among the 247 surveyed was not
486 significantly direction selective at any velocity. This result demonstrates that neurons were
487 nearly universally direction selective to chirps in aperiodic stimuli.

488 As for the SCHR ROC analysis, responses to each chirp-direction pair were shuffled for
489 each neuron, and an ROC test was performed on the shuffled responses to ensure that a
490 reasonable threshold was used for determining direction selectivity. Shuffling the responses
491 1000 times, 13.3% of the neurons were selective for at least one F0/C condition (with a
492 standard deviation of 9.0%). It is clear that the actual percentage of 99.6% could not be due to
493 variance in the data, suggesting that the threshold used in the ROC test (70.07%) was
494 sufficiently high.

495 **E.** Prevalence and direction of ARC selectivity were related to chirp velocity, but not MTF
496 shape or CF

497 The results of ROC analysis revealed different trends for ARC and SCHR responses. As
498 expected, there was not as pronounced an effect of MTF shape on either the prevalence or
499 direction of ARC selectivity (Fig. 10). BE-neuron selectivity was not more prevalent than that of
500 other MTF shapes, as seen in Fig. 8. Instead, all MTF shapes showed decreasing prevalence of
501 direction selectivity with increasing chirp velocity (Table 2). Direction of ARC selectivity changed
502 with chirp velocity as well – at the two slower velocities tested (±0.40 and ±0.80 kHz/ms),
503 neurons were more frequently selective for positive chirp velocities (blue, equivalent to −SCHR).
504 At the four higher velocities (±1.59 kHz/ms and faster), neurons of all MTF types were more
505 likely to be selective for negative velocities (red, equivalent to +SCHR).

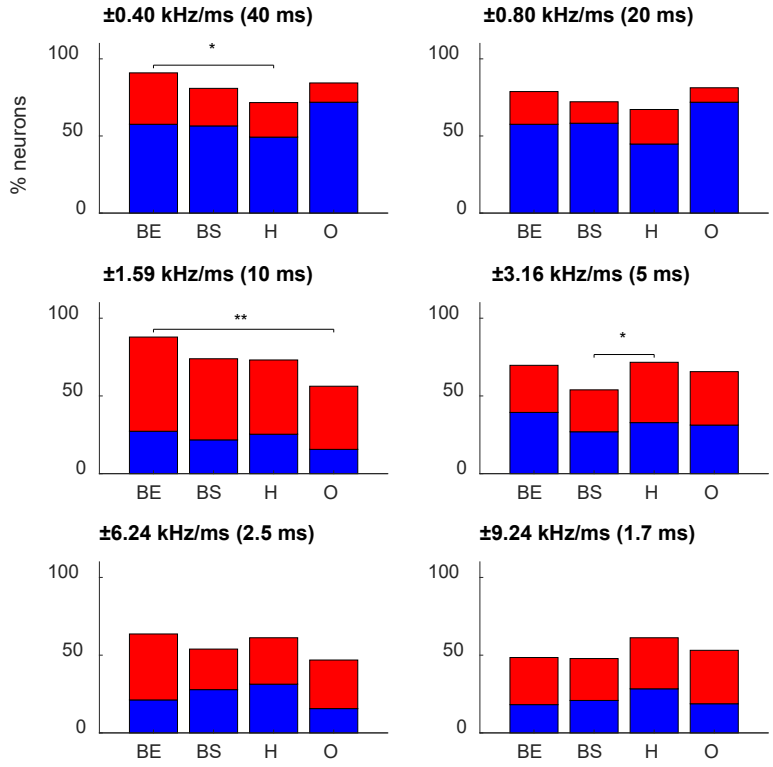

Figure 10 - Percent of direction selective neurons determined by ROC analysis for different MTF shapes, by ARC chirp duration (BE – Band-Enhanced, BS – Band-Suppressed, H – Hybrid, O – Other). In terms of chirp velocity, an ARC chirp of ±0.80 kHz/ms has a duration of 20 ms (equivalent to a SCHR chirp F0 of 50 Hz), ±1.59 kHz/ms has a duration of 10 ms (SCHR F0 100 Hz, etc.). Blue bar-segments correspond to upward-selective neurons (equivalent to −SCHR), and red bar-segments correspond to downward-selective neurons (equivalent to +SCHR). Brackets indicate significant differences of direction selectivity prevalence between groups, as determined by the χ^2 test of independence, with asterisks indicating the level of significance ($p < 0.05$, ** $p < 0.01$, *** $p < 0.001$). Precise p-values are reported here for each panel. ±0.40 kHz/ms (40 ms)—BE-H, $p = 0.0287$. ±1.59 kHz/ms (10 ms)—BE-O, $p = 0.0044$. ±3.16 kHz/ms (5 ms)—BS-H, $p = 0.0183$.*

The trends observed for direction selectivity in neurons with different MTF types were also observed for CF groups (Fig. 11). CF was not strongly related to the prevalence nor the direction of ARC selectivity; rather, prevalence of direction sensitivity in all CF groups decreased

with increasing chirp velocity. Also, neurons were more commonly selective for chirps of negative velocity (+SCHR) at higher chirp velocities.

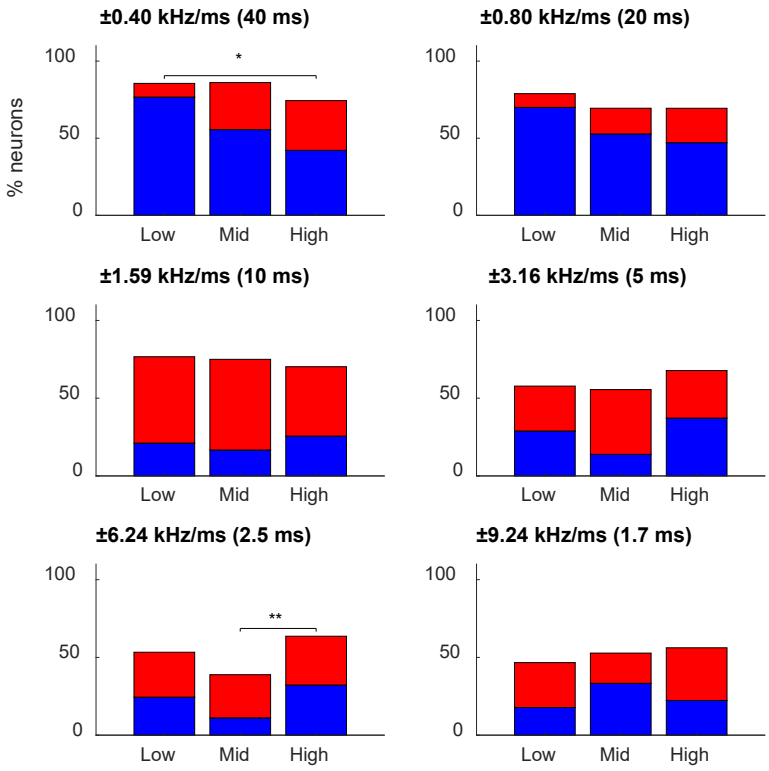

Figure 11 - Percent of direction selective neurons determined by ROC analysis for different CF ranges, low (<3 kHz), mid (>3 kHz and <6 kHz), and high (>6 kHz), by ARC chirp. In terms of chirp velocity, an ARC chirp of ±0.80 kHz/ms has a duration of 20 ms (equivalent to a SCHR chirp F0 of 50 Hz), ±1.59 kHz/ms has a duration of 10 ms (SCHR F0 100 Hz, etc.). Blue bar-segments correspond to upward-selective neurons (equivalent to −SCHR), and red bar-segments correspond to downward-selective neurons (equivalent to +SCHR). Brackets indicate significant differences of direction selectivity prevalence between groups, as determined by the χ^2 test of independence, with asterisks indicating the level of significance ($p < 0.05$, ** $p < 0.01$, *** $p < 0.001$). Precise p-values are reported here for each panel. ±0.40 kHz/ms (40 ms)—Low-High, $p = 0.0481$. ±6.24 kHz/ms (2.5 ms)—Mid-High, $p = 0.0083$.*

F. RVFs were often direction selective at slower-velocities and direction-insensitive at higher-velocities

In order to determine which response properties were the most common, principal component analysis (PCA) was performed on the set of RVFs. Figure 12 shows the first three principal components, which together explained 74.0% of the variance in the data. Principal component 1 (PC1) had relatively high weights at high-magnitude velocities, showing that rate responses to high velocities tended to be positively correlated, regardless of direction. PC1 explained 48.5% of variance in the RVF data. Principal component 2 (PC2) had high weights at low-magnitude velocities, showing that rate responses to low velocities also tended to be positively correlated, regardless of direction. PC2 explained 13.8% of variance in the data. Finally, PC3 had large positive weights at positive, slow velocities and negative weights at negative, slow velocities, demonstrating that responses to positive and negative velocity chirps tended to be negatively correlated at slow velocities. PC3 was the main PCA dimension reflecting direction selectivity. PC3 explained 11.7% of variance in the data.

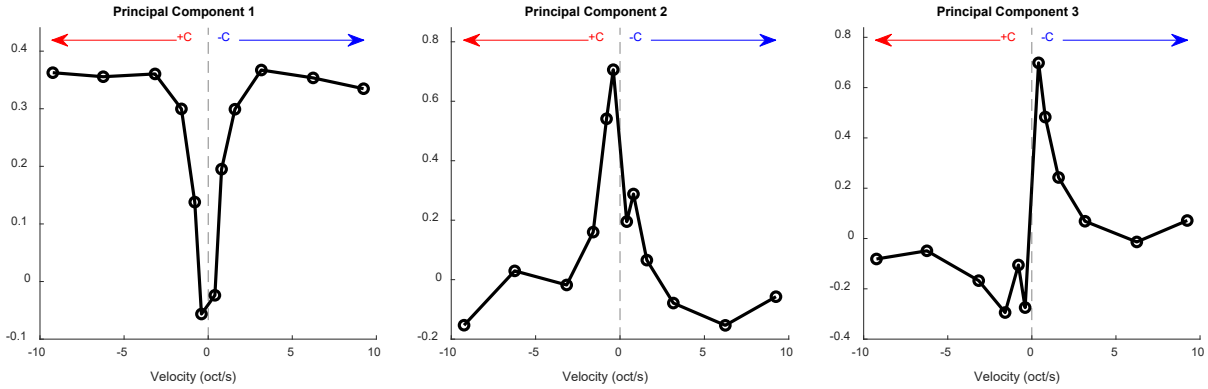

Figure 12 – Principal components derived from the set of RVFs (left, PC1; center, PC2; right, PC3). Y-axes reflect principal-component weights and are unitless.

The shapes of the first three principal components of the RVF data suggest that the most salient features of a neuron's RVF were its responses to high- and low-velocity chirps,

rather than the direction of those chirps. However, PC3 showed that the direction selectivity of neurons for low-velocity chirps was an important feature of these datasets—however, PC3 primarily represented low-velocity chirp direction selectivity, consistent with the observation that chirp-direction selectivity at high-velocities was not as common. Instead, neural responses to chirps of high velocities tended to depend on absolute velocity rather than on direction.

As shown in Fig. 13, there was not a clear relationship between the scores of principal components 1-3 and either MTF type (symbol shapes) or CF (symbol colors). This result suggested that RVFs could not be simply derived from MTFs or CFs. Furthermore, based on the three scatter plots in Fig. 13, there were no clusters of neurons based on principal-component analysis – that is, RVF subgroups were not revealed by this analysis.

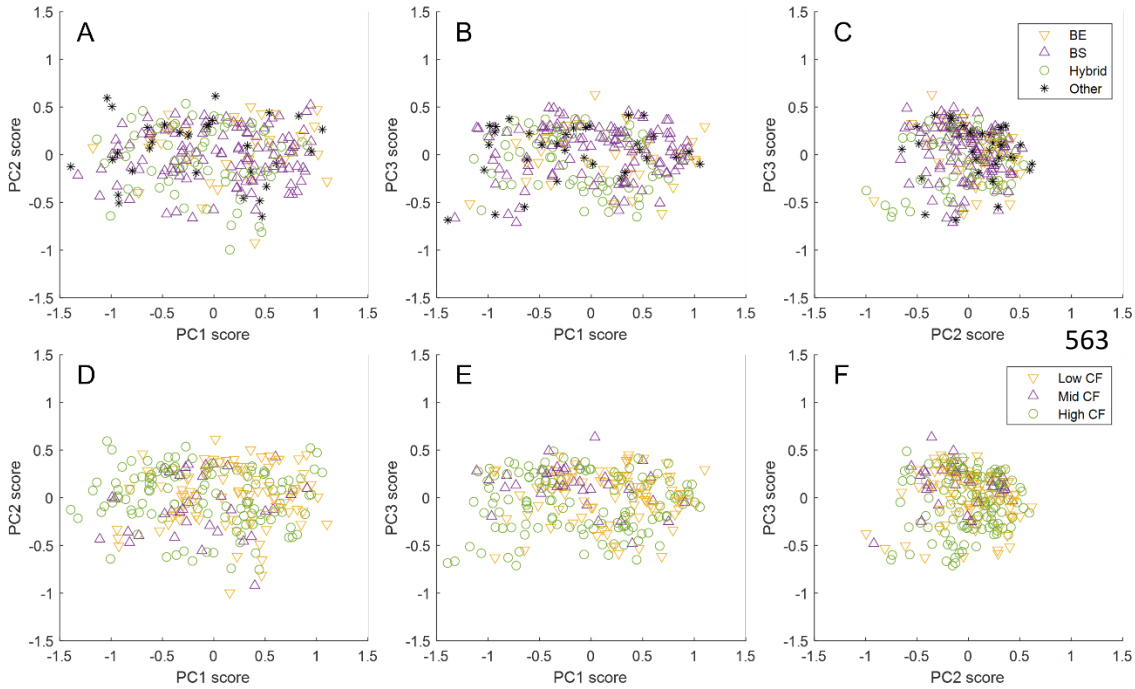

Figure 13 – Scatter plots depicting the Principal Component scores of each neuron, organized by MTF shape (A-C) and CF range (D-F). (A and D, PC2 vs PC1; B and E, PC3 vs PC1; C and F, PC3 vs PC2). In the top row (A-C), BE neurons are represented by yellow upward triangles, BS neurons by purple downward triangles, hybrid neurons by green circles, and other MTF shapes by black asterisks. In the bottom row (D-F), Low-CF neurons are represented by yellow upward triangles, mid-CF by purple downward triangles, and high-CF by green circles.

572 **G**. Velocity cues facilitated predictions of SCHR rate

573 Starting from the premise that responses to SCHR stimuli are dependent on AM
574 (periodicity) tuning and/or velocity tuning, we used MTFs and ARC responses to predict SCHR
575 responses using a GLM. Figure 14 shows a visualization of this strategy on an example neuron
576 (R24TT2P8N4, also depicted in Fig. 4). The neuron's SCHR response is shown as a surface
577 plot on periodicity-velocity axes; darker colors correspond to higher response rates. This neuron
578 responded more strongly to lower F0s and to +SCHR (Fig. 14A). The color bars above and to
579 the left of the SCHR surface are the MTFN and ARC responses of the neuron, respectively, and
580 describe how the neuron's response rate depended on periodicity or velocity alone. Using a
581 weighted combination of these two responses, the GLM predicted the SCHR response (Fig.
582 14B). By fitting an equation that included both periodicity and velocity terms (Eqn. 1), an
583 accurate prediction of the recorded SCHR data was made ($R^2 = 0.98$). Removing either the
584 periodicity or velocity terms reduced the quality of the prediction (Fig. 14C, D) (note that their
585 interaction will be examined below). Predicting the SCHR response using the periodicity-only
586 model (Eqn. 2) resulted in the disappearance of the distinct direction selectivity at lower F0s
587 (Fig. 14C). Notably, a model using only periodicity tuning could not explain the observed
588 direction selectivity. Conversely, a prediction of the SCHR responses using the velocity-only
589 model (Eqn. 3) explained a relatively small amount of variance in the data ($R^2 = 0.25$). This
590 neuron was typical in that more variance in the data was explained by the periodicity-only model
591 than by the velocity-only model. However, this neuron was also typical in that the velocity terms
592 contribute a substantial percentage of the variance explained by the combined model, as
593 compared to the periodicity-only model.

594 The RVF in Fig. 14 had a higher response rate for downward sweeps (+SCHR).
595 However, this neuron was only selective for +SCHR at low F0s. Figure 15 shows how the
596 velocity cue was used differently by the combined GLM model depending on periodicity. For

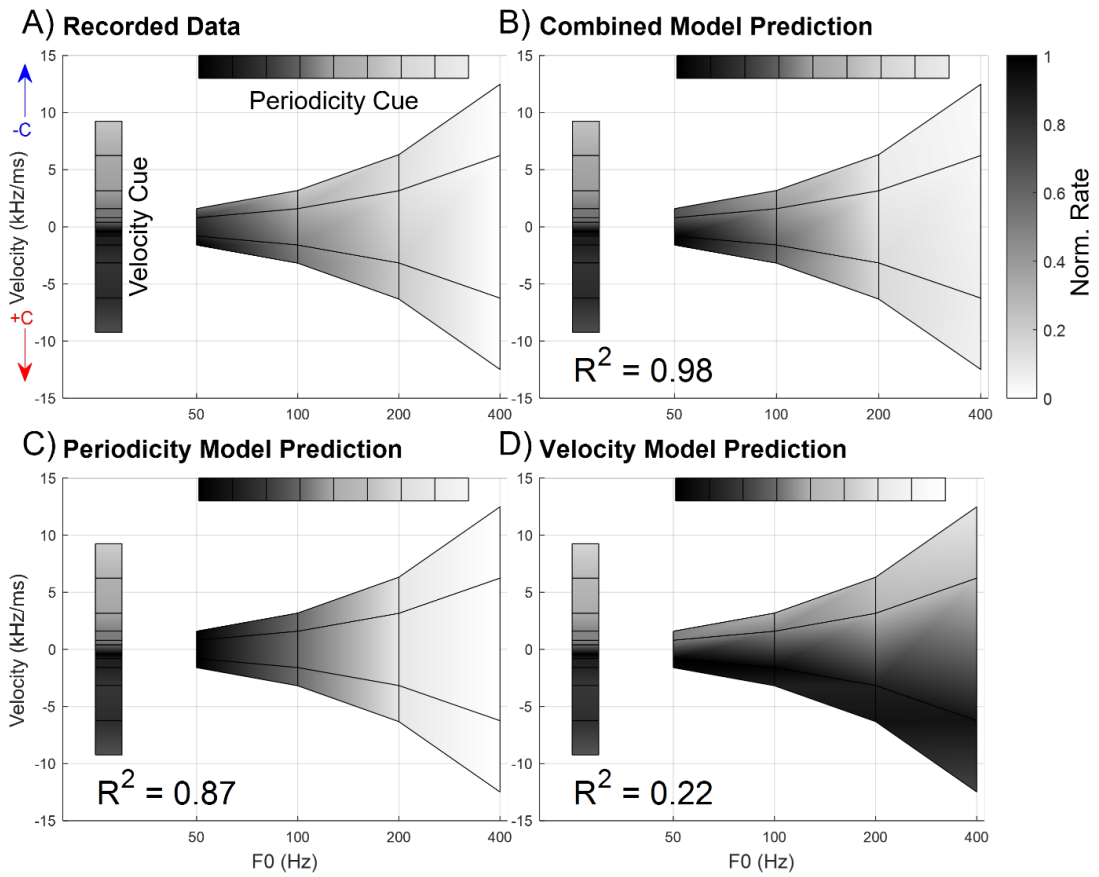

Figure 14 – GLM prediction of SCHR rates for an example neuron (R24TT2P8N4; same neuron as in Fig. 4). (A) SCHR rates plotted in Periodicity-Velocity space (center surface). Each of the 16 points on the surface plot correspond to an individual SCHR F0/C-value combination – for instance, four points have a SCHR F0 of 50 Hz. Their velocities vary with C-value; the points' C-values, from top to bottom, are -0.5, -1, 1, 0.5. This surface plot demonstrates the effect of C-value on chirp velocity. The periodicity cue and velocity cue are plotted alongside the SCHR surface plot—these are the MTF and RVF, respectively. The modulation frequency range of the MTF was limited to the section relevant to the range of SCHR F0s (50 – 400 Hz). Rate is marked using color, with darker shades indicating larger rates. The rate scale of each surface plot is separately normalized by its own maximum rate—thus, shading does not reflect absolute rates. Surface plot colors are interpolated. (B) SCHR rates predicted using the combined GLM equation (Eqn. 1), which uses both periodicity and velocity cues. Coefficient of determination (R^2) between predicted and recorded SCHR rates is also shown. (C) SCHR rates predicted using the periodicity-only GLM equation (Eqn. 2), and corresponding R^2-value. (D) SCHR rates predicted using the velocity-only GLM equation (Eqn. 3), and corresponding R^2-value.

ARC velocities that closely matched the velocities of SCHR chirps with F0 equal to 50 Hz, a large change in ARC rate was associated with a high predicted SCHR rate (blue line). For higher F0s, ARC rate had a smaller impact on the predicted SCHR rate, with SCHR-ARC-line slopes approaching zero (200- and 400-Hz lines, yellow and purple). Therefore, despite the RVF suggesting a strong selectivity for downward sweeps at all velocities, Fig. 15 shows that the interaction between velocity and periodicity sensitivities drove the SCHR response rates. The importance of velocity-periodicity interaction illustrated in Fig. 15 was typical of many neurons in the study.

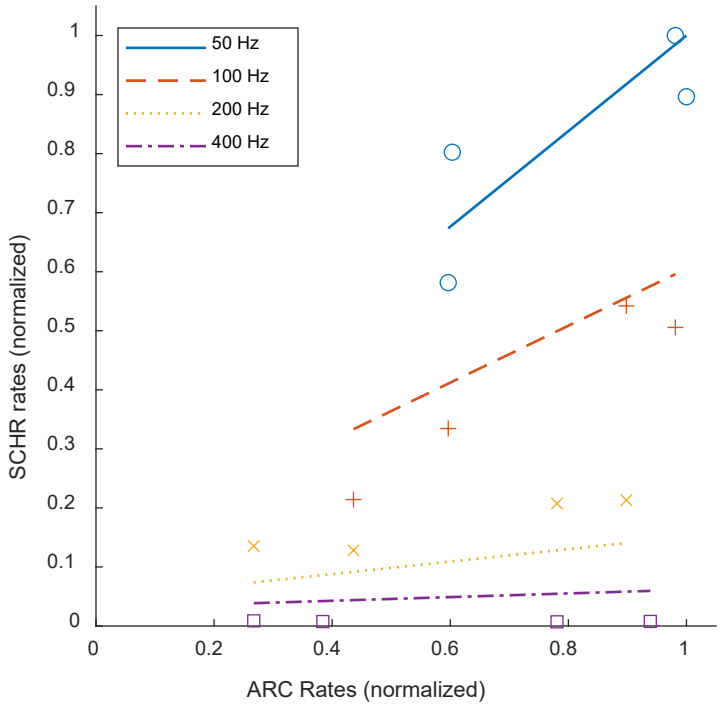

Figure 15 – SCHR rates vs ARC rates (velocity cue) of unit R24TT2P8N4 plotted as recorded data (scatter plot) and GLM-fitted lines (solid lines). Blue solid line and circles correspond to 50 Hz, orange dashed line and plus signs correspond to 100 Hz, yellow dotted line and crosses correspond to 200 Hz, and purple dash-dotted line and squares correspond to 400 Hz. Both SCHR and ARC rates are normalized by their own maximum rate. This example neuron is also shown in Figs. 4 and 14.

Using the method outlined in Fig. 14, an R^2 value was obtained for each of the three GLM models (Eqns. 2-4) by comparing predictions to neural responses. The contribution of velocity terms to the total explainable variance was calculated as a percentage, using Eqn. 4. Figure 16 shows this percentage versus the variance explained by the combined model. Many symbols are clustered around the *x*-axis, indicating that the contribution of velocity was not the primary determinant of SCHR rate and that periodicity tuning was the more important feature in predicting SCHR responses for these neurons. However, for neurons with a high total variance explained by the combined model (80-100%), the average contribution of velocity terms was about 20% and ranged up to about 50%. Figure 14 shows an example of such a neuron with high total explainable variance; the relatively small contribution of velocity to the predictions was not insubstantial because it necessarily contained all information about direction selectivity, a cue for which the example unit was clearly sensitive (Fig. 4D, RVF). Furthermore, for many neurons with relatively low (20-60%) total explainable variance, the contribution of the velocity terms explained over 50% of the explained variance, suggesting that velocity cues were important predictors of these SCHR responses, perhaps more so than the relatively weaker periodicity predictor.

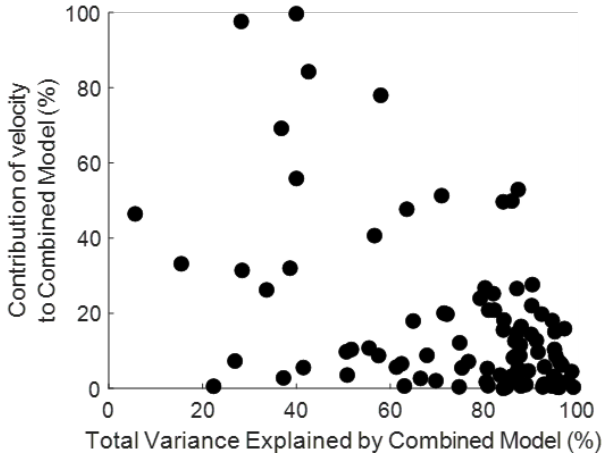

Figure 16 - A. (left) Percent variance explained in the SCHR response using the ARC model alone versus percent variance explained by the combined model. B. (right) Percent contribution of the ARC terms to the total explainable variance by the combined model vs. Variance explained by the combined model.

645 In summary, direction selectivity between SCHR pairs could not be explained with a
646 model using periodicity alone. Because SCHR-direction selectivity was common (90.5%, Table
647 1), most IC neuron responses were necessarily influenced by velocity sensitivity.

648 **Discussion**

649 This study demonstrated the diversity of sensitivity to the velocity and direction of fast
650 frequency chirps in the IC, for the first time in an awake-rabbit model. Using ROC analysis, IC
651 neurons were shown to be commonly selective for SCHR chirp direction, with 90.5% of neurons
652 surveyed selective for at least one condition (Table 1). Neurons were also nearly universally
653 selective for chirp direction in response to the novel ARC stimulus (Table 2). This study also
654 showed that individual neurons had a wide variety of rate-response profiles which were
655 described using RVFs. RVFs revealed that neurons were more commonly direction selective to
656 chirps of lower velocities and responded to higher velocities in a direction-insensitive way.
657 Finally, GLM analysis was performed to show that in many cases SCHR rates could be
658 accurately reconstructed using the periodicity and velocity sensitivity reflected in MTFs and
659 RVFs, respectively. The combination of both velocity and periodicity cues was necessary to
660 achieve the best model predictions.

661 A common use of Schroeder-stimuli has been as a masker in psychophysical
662 experiments evaluating detection of an increment in tone level. Notably, there is an effect of
663 Schroeder-phase on its effectiveness as a masker, with up to 20-dB lower thresholds (less
664 masking) for +SCHR maskers than for −SCHR maskers (Smith et al., 1986). An explanation
665 from the literature attributes this effect to asymmetry of filtering in the cochlea—phase-
666 dispersive properties of the basilar membrane (BM) result in a peakier response profile for
667 +SCHR than −SCHR, which is then compressed at the output of the cochlea, resulting in higher
668 average energy in −SCHR BM responses compared to +SCHR, and thus more effective
669 masking by -SCHR stimuli (Recio and Rhode, 2000; Summers et al., 2003). This logic can also

be applied to explain rate-differences between SCHR C-values. However, the results here suggest that other factors underlie the widespread chirp selectivity of IC single-units observed in this study. First, the phase-dispersion of the BM depends on CF, with neural masking differences observed primarily for CFs > 3-4 kHz (Recio, 2001). In this study, no consistent differences were observed in either the prevalence or direction of chirp selectivity between low-CF (< 3 kHz) and mid- or high-CF (> 3 kHz) neurons, in either SCHR or ARC rates (Figs. 9, 11). Secondly, the cochlear dispersion hypothesis can only explain SCHR selectivity towards −SCHR; despite this, neurons in the mid-to-high-CF range (> 3 kHz) could be selective for either positive or negative SCHR stimuli (Fig. 9), suggesting that cochlear phase-dispersion was not the basis of IC chirp sensitivity. Similarly, Henry et al. (2022) found diverse SCHR selectivity in the IC of budgerigars (parakeet), though a statistical gradient was observed from −SCHR selectivity at CFs below 2-3 kHz to +SCHR selectivity for higher CFs. These findings were also consistent with a recent study in gerbils (Steenken et al., 2022) which reported that average rates of AN fibers could not explain behavioral discrimination of SCHR stimuli in gerbils, whereas temporal analyses of AN responses over short time (1-ms) windows could explain behavioral thresholds. Low correlations of AN rate to behavior provides further evidence against cochlear phase-dispersion driving IC selectivity. On the other hand, the presence of information for SCHR direction discrimination in the relatively fine timing of AN fibers is consistent with neural mechanisms that combine temporal information across frequency channels.

A potential mechanism to explain the diverse chirp-response profiles seen in this study may be found in IC inhibition. IC neurons receive excitatory and inhibitory inputs with varying frequencies and latencies that may interact to produce chirp selectivity (Pollak et al., 2011). Interactions between excitatory and inhibitory inputs varying in latency have long been implicated in mechanisms for frequency-sweep selectivity in bats (Suga, 1965; Fuzessery and Hall, 1996; Gordon and O'Neill, 1998). These mechanisms broadly are dependent on sideband

695 inhibitory regions in excitatory tuning curves and the resulting asymmetry of responses to
696 upward and downward frequency sweeps. Although not directly observed for all neurons, RM
697 inhibition did not reliably predict chirp-direction selectivity among neurons for which inhibition
698 was observed (e.g. Fig. 3), suggesting that sideband inhibition is not the sole mechanism
699 underlying selectivity. To more comprehensively assess the effect of inhibition on chirp
700 sensitivity, inhibition in the IC could be assessed by measuring RMs using pure tones in
701 background noise – this would be an interesting direction for a future study.

702 A related mechanism for chirp selectivity based on dendritic filtering was proposed by
703 Rall (1969) who included excitatory inputs organized spatially by frequency. In Rall's framework,
704 a sweep that activates distal dendrites first, and proximal dendrites later, would temporally sum
705 and generate a large synaptic input. While the existence of such large dendritic fields has not
706 been reported in the IC, this mechanism has been hypothesized to underlie the FM directionality
707 of octopus cells in the posteroventral cochlear nucleus (Rhode and Greenberg, 1992; Pollak et
708 al., 2011). Notably, octopus cells project to the VNLL, which provides inhibitory innervation to
709 the IC (Adams, 1997; Vater et al., 1997; Winer et al., 1995). Thus, FM directionality of octopus
710 cells, by way of the VNLL, may explain chirp selectivity in the IC; in this scenario, responses to
711 chirps in one direction would be inhibited by input from the VNLL and disinhibited by chirps in
712 the opposite direction. The possibility that IC chirp sensitivity originates in octopus cells is
713 particularly intriguing because, like IC neurons, octopus cells display a diversity of chirp
714 response profiles and can be selective to either upward or downward chirps (Lu et al., 2022).
715 Note that Lu et al. (2022) suggested that the diverse chirp selectivity in octopus cells could be
716 explained by sequence detection, with excitation determined by a sequence of inputs with both
717 frequency-dependent delays and varied amplitudes, rather than by simple coincidence detection
718 of inputs with frequency-dependent delays.

Sensitivity to the direction of fast frequency changes has also been evaluated using neural responses to stimuli with random spectrotemporal fluctuations. One example is the Dynamic Moving Ripple (DMR) stimulus described in Escabí and Schreiner (2002). Designed to mimic spectrotemporal modulations present in natural sounds, such as speech or animal vocalizations, the stimulus is composed of a bank of sinusoidal carriers with an imposed spectrotemporal envelope. DMR stimuli have been used to generate spectrotemporal receptive fields (STRFs), which describe how neural response properties vary over frequency and time. It should be possible to produce a DMR stimulus with ripple velocity equivalent to SCHR chirps by substantially increasing the velocity of frequency sweeps compared to the original DMR stimuli. Doing so would require careful co-modulation of the temporal and spectral modulation variables and selection of an appropriate temporal analysis window for computing the stimulus spectrogram, which would be necessary to generate temporally-informative STRFs. Such STRFs may provide additional clues for analyzing IC neurons' chirp tuning.

While the combined GLM with both periodicity and velocity cues was able to reproduce SCHR rate profiles of IC neurons, often with high accuracy, some predictions did not explain a high percentage of the variance (Fig. 16), suggesting that additional factors shaping SCHR rate profiles have yet to be uncovered. One possible source of this discrepancy was a gradual change in rate over long (50 – 150 ms) durations—Fig. 3 shows an example in which rate gradually increased (100 Hz F0), and Fig. 7 shows an example in which rate gradually decreased (50 Hz F0, C = -1). These long-term effects may be attributable to the auditory efferent system, and cannot be captured using the brief ARC stimulus. Similar long-term changes in rate have been reported in response to other complex sounds, representing a possible direction for future research (Farhadi et al., 2021).

SCHR-chirp sensitivity in the IC suggests a mechanism that may influence midbrain-level encoding of speech. When speech sounds, or any animal vocalizations, are produced,

resonances within the vocal tract act as second-order filters, introducing phase shifts between components of harmonic sounds (Klatt, 1980). In the same way that SCHR chirps are produced by the relative phases of harmonic components, vocalizations will contain chirp-like features to which IC neurons may be similarly sensitive. IC neurons in this study were sensitive to SCHR chirps and directions over a frequency range relevant to human speech. Close examination of IC responses to SCHR chirps may reveal a novel influence on midbrain responses that is relevant to neural coding of speech and other harmonic sounds. The interaction of periodicity tuning and frequency-sweep velocity sensitivity observed in this study would also influence responses to other complex harmonic sounds, such as those common in speech and music.

Acknowledgements

We acknowledge the assistance of Kristina S. Abrams, Johanna B. Fritzinger, and Dr. Swapna Agarwalla for help with physiological experiments. Supported by NIH-DC001641 and NIH-F31DC019816.

References

Adams JC (1997) Projections from octopus cells of the posteroventral cochlear nucleus to the ventral nucleus of the lateral lemniscus in cat and human. Aud Neurosci 3:335-350.

Andoni S, Li N, Pollak GD (2007) Spectrotemporal Receptive Fields in the Inferior Colliculus Revealing Selectivity for Spectral Motion in Conspecific Vocalizations. The Journal of Neuroscience 27:4882-4893.

Awan SN, Novaleski CK, Rousseau B (2014) Nonlinear Analyses of Elicited Modal, Raised, and Pressed Rabbit Phonation. Journal of Voice 28:538-547.

Casseday JH, Ehrlich D, Covey E (1994) Neural Tuning for Sound Duration: Role of Inhibitory Mechanisms in the Inferior Colliculus. Science 264:847-850.

767 Davis KA (2005) Spectral Processing in the Inferior Colliculus. In: International Review of
768 Neurobiology, pp 169-205: Academic Press.

769 Egan JP, Egan JP (1975) Signal detection theory and ROC-analysis: Academic press.

770 Escabi MA, Schreiner CE (2002) Nonlinear spectrotemporal sound analysis by neurons in the
771 auditory midbrain. Journal of Neuroscience 22:4114-4131.

772 Escabi MA, Miller LM, Read HL, Schreiner CE (2003) Naturalistic auditory contrast improves
773 spectrotemporal coding in the cat inferior colliculus. Journal of Neuroscience 23:11489-11504.

774 Farhadi A, Jennings SG, Strickland EA, Carney LH (2021) A Closed-Loop Gain-Control
775 Feedback Model for The Medial Efferent System of The Descending Auditory Pathway. In:
776 ICASSP 2021 - 2021 IEEE International Conference on Acoustics, Speech and Signal
777 Processing (ICASSP), pp 291-295.

778 Fuzessery ZM (1994) Response selectivity for multiple dimensions of frequency sweeps in the
779 pallid bat inferior colliculus. Journal of Neurophysiology 72:1061-1079.

780 Fuzessery Z, Hall J (1996) Role of GABA in shaping frequency tuning and creating FM sweep
781 selectivity in the inferior colliculus. Journal of neurophysiology 76:1059-1073.

782 Gordon M, O'Neill WE (1998) Temporal processing across frequency channels by FM selective
783 auditory neurons can account for FM rate selectivity. Hearing research 122:97-108.

784 Heffner H, Masterton B (1980) Hearing in Glires: Domestic rabbit, cotton rat, feral house mouse,
785 and kangaroo rat. The Journal of the Acoustical Society of America 68:1584-1599.

786 Henry KS, Wang Y, Abrams KS, Carney LH (2023) Mechanisms of masking by Schroeder-
787 phase harmonic tone complexes in the budgerigar (*Melopsittacus undulatus*).
788 bioRxiv:2022.2010.2026.513930.

789 Kim DO, Carney L, Kuwada S (2020) Amplitude modulation transfer functions reveal opposing
790 populations within both the inferior colliculus and medial geniculate body. Journal of
791 Neurophysiology 124:1198-1215.

792 Klatt DH (1980) Software for a cascade/parallel formant synthesizer. The Journal of the
793 Acoustical Society of America 67:971-995.

794 Krishna BS, Semple MN (2000) Auditory Temporal Processing: Responses to Sinusoidally
795 Amplitude-Modulated Tones in the Inferior Colliculus. Journal of Neurophysiology 84:255-273.

796 Langner G, Schreiner CE (1988) Periodicity coding in the inferior colliculus of the cat. I.
797 Neuronal mechanisms. Journal of Neurophysiology 60:1799-1822.

798 Levitt H (1971) Transformed up-down methods in psychoacoustics. The Journal of the
799 Acoustical society of America 49:467-477.

800 Liberman AM, Mattingly IG (1989) A Specialization for Speech Perception. Science 243:489-
801 494.

802 Lu H-W, Smith PH, Joris PX (2022) Mammalian octopus cells are direction selective to
803 frequency sweeps by excitatory synaptic sequence detection. Proceedings of the National
804 Academy of Sciences 119:e2203748119.

805 Nelder JA, Wedderburn RW (1972) Generalized linear models. Journal of the Royal Statistical
806 Society: Series A (General) 135:370-384.

807 Nelson PC, Carney LH (2007) Neural Rate and Timing Cues for Detection and Discrimination of
808 Amplitude-Modulated Tones in the Awake Rabbit Inferior Colliculus. Journal of Neurophysiology
809 97:522-539.

810 Pollak GD, Xie R, Gittelman JX, Andoni S, Li N (2011) The dominance of inhibition in the inferior
811 colliculus. Hearing Research 274:27-39.

Rall W (1969) Time constants and electrotonic length of membrane cylinders and neurons. Biophysical Journal 9:1483-1508.

Recio A (2001) Representation of harmonic complex stimuli in the ventral cochlear nucleus of the chinchilla. The Journal of the Acoustical Society of America 110:2024-2033.

Recio A, Rhode WS (2000) Basilar membrane responses to broadband stimuli. The Journal of the Acoustical Society of America 108:2281-2298.

Rhode WS, Greenberg S (1992) Physiology of the cochlear nuclei. In: The mammalian auditory pathway: Neurophysiology, pp 94-152: Springer.

Schroeder M (1970) Synthesis of low-peak-factor signals and binary sequences with low autocorrelation (Corresp.). IEEE Transactions on Information Theory 16:85-89.

Schwarz DM, Zilany MSA, Skevington M, Huang NJ, Flynn BC, Carney LH (2012) Semi-supervised spike sorting using pattern matching and a scaled Mahalanobis distance metric. Journal of Neuroscience Methods 206:120-131.

Smith BK, Sieben UK, Kohlrausch A, Schroeder MR (1986) Phase effects in masking related to dispersion in the inner ear. The Journal of the Acoustical Society of America 80:1631-1637.

Steenken F, Oetjen H, Beutelmann R, Carney LH, Koeppl C, Klump GM (2022) Neural processing and perception of Schroeder-phase harmonic tone complexes in the gerbil: Relating single-unit neurophysiology to behavior. European Journal of Neuroscience 56:4060-4085.

Suga N (1965) Analysis of frequency-modulated sounds by auditory neurones of echo-locating bats. J Physiol 179:26-53.

Summers V, Boer Ed, Nuttall AL (2003) Basilar-membrane responses to multicomponent (Schroeder-phase) signals: Understanding intensity effects. The Journal of the Acoustical Society of America 114:294-306.

835 Vater M, Covey E, Casseday J (1997) The columnar region of the ventral nucleus of the lateral
836 lemniscus in the big brown bat (Eptesicus fuscus): synaptic arrangements and structural
837 correlates of feedforward inhibitory function. Cell and tissue research 289:223-233.

838 Whitehead ML, Lonsbury-Martin BL, Martin GK (1992) Evidence for two discrete sources of
839 2f1−f2 distortion-product otoacoustic emission in rabbit: I. Differential dependence on stimulus
840 parameters. The Journal of the Acoustical Society of America 91:1587-1607.

841 Winer JA, Larue DT, Pollak GD (1995) GABA and glycine in the central auditory system of the
842 mustache bat: structural substrates for inhibitory neuronal organization. Journal of Comparative
843 Neurology 355:317-353.

844 Yin TCT, Smith PH, Joris PX (2019) Neural Mechanisms of Binaural Processing in the Auditory
845 Brainstem. Compr Physiol 9:1503-1575.